Composites Part C: Open Access 19 (2026) 100700

Contents lists available at ScienceDirect

Composites Part C: Open Access

journal homepage: www.sciencedirect.com/journal/composites-part-c-open-access

Introducing Legendre wavelet functions for damage detection in laminated composite beams

Morteza Saadatmorad [a,b], Nicholas Fantuzzi [a,b,*], Pietro Russo [c]

[a] Department of Civil, Chemical, Environmental and Materials Engineering, University of Bologna, Viale del Risorgimento 2, 40136 Bologna, Italy
[b] Department of Civil, Chemical, Environmental and Materials Engineering, University of Bologna, Via Tombesi Dall'Ova 55, Ravenna 48121, Italy
[c] Institute for Polymers, Composites and Biomaterials – National Research Council, Via Campi Flegrei 34, Pozzuoli, NA 80078, Italy

ARTICLE INFO

Keywords:
Legendre wavelet functions
Damage detection
Laminated composite beams
Wavelet transform
Damaged structures

ABSTRACT

This paper introduces Legendre wavelets as a novel wavelet type and explores their effectiveness in detecting damage in carbon-epoxy composite beams. These wavelets are generated by differentiating the first derivative of Legendre functions on a ten-digit grid using finite difference methods, resulting in three versions with seven, five, and three sampling points. The Legendre wavelet functions with five and three sampling points are computed. Carbon-epoxy laminated composite beam mode shapes serve as the input signal for a Legendre wavelet transform. Numerical and experimental studies validate the practical applicability of these wavelets for damage detection. Results demonstrate that all Legendre wavelet functions are suitable for damage detection in laminated composite beams. Especially, those derived from higher-degree Legendre polynomials exhibit superior performance.

1. Introduction

Early damage detection is crucial for extending structural lifespan and ensuring proper maintenance [1]. While various Structural Health Monitoring (SHM) methods exist, each with unique advantages and disadvantages, they generally fall into two categories: local methods, which monitor specific areas, and vibration-based methods, known as global methods, which assess the structure as a whole [2–5]. A suitable SHM method is to combine a vibration-based method with one or more other local methods [6]. Thus, the vibration-based method is a supportive method for local SHM methods [7–10].

Following structural health monitoring (SHM) to detect damage, damage detection methods locate and classify the damage to inform repair decisions. Vibration-based methods are a key approach among available damage detection techniques. Vibration-based damage detection methods use either natural frequencies or mode shapes to discover the location of damage in structures [11]. When natural frequencies are used to detect damage location, many natural frequencies corresponding to various damage locations are required [12–14]. Typically, damage location is estimated using optimization or machine learning techniques by inputting the natural frequencies of a damaged structure, often requiring prior knowledge of both intact and various damaged states [15–19]. However, acquiring such extensive frequency data is often impractical. In contrast, Mode shapes provide a practical and simplified approach to identifying vibration damage. Obtaining the structure's mode shapes, which inherently contain damage information, is often sufficient [20]. If direct observation is inconclusive, signal processing techniques can be used to locate the damage [21].

Processing the mode shapes for detecting damage can be performed using various methods [22–25]. To date, multiple researchers have proposed different methods for mode shape-based damage detection. For example, Duvnjak et al. [26] investigated the Mode Shape Damage Index (MSDI) for detecting isolated damage in reinforced concrete (RC) slabs. Based on the difference in modified modal displacements between intact and damaged states, the method was evaluated through experimental modal analysis on an RC slab subjected to ten damage scenarios, varying in quantity, severity, and boundary conditions. The MSDI effectively detects the presence, location (single or multiple), and severity of single, isolated damage cases. Umar et al. [27] proposed a response surface modeling (RSM) method for structural damage detection that utilizes both natural frequencies and mode shapes, addressing the shortcomings of traditional frequency-based methods. Numerical and experimental validation using a simply supported beam and a laboratory steel frame indicated the potential of RSM for damage detection.

* Corresponding author.
E-mail address: nicholas.fantuzzi@unibo.it (N. Fantuzzi).

https://doi.org/10.1016/j.jcomc.2026.100700

Available online 26 January 2026

Wavelet transform, a signal processing method capable of transforming signals from the time or space domain to the time-frequency or space-frequency domain, is a popular technique for detecting structural damage using mode shape [28–29]. Its ability to identify local disruptions in signal frequency caused by damage at specific times or locations has made it widely adopted for this purpose [30]. Yang et al. [31] established the theoretical basis for the modal frequency curve method and demonstrated the extraction of defect and damage features from the frequency curve using wavelet decomposition. Building on this, a novel damage index, based on multimodal wavelet squares residuals, was presented along with a damage size estimator derived from its standard deviation. The proposed damage index offered more robust and clearer damage identification compared to existing methods. Saadatmorad et al. [32] presented a novel method to process mode shape signal using one-dimensional continuous wavelet transform (1D-CWT). They proposed a damage detection technique for reinforced laminate composite beams. The method used the covariance of mode shapes as the input signal of CWT to improve the accuracy of damage detection. Papanaboina et al. [33] improved delamination detection in CFRP using numerical modeling to optimize the zero-mode asymmetric guided wave. The defect location was estimated using the signal time of flight, with the continuous wavelet transform (CWT) outperforming the Hilbert transform in accuracy. Delamination depth was determined by analyzing signal strength across frequency ranges. The study suggested the inverse fast Fourier transform for wave reconstruction to enhance signal clarity and interpretation. The discrete wavelet transform (DWT) is widely used for structural damage detection because the continuous wavelet transform (CWT) suffers from redundancy at higher scales [34]. Ravanfar et al. [35] presented a vibration-based damage detection method for beam-like structures. Their method used entropy analysis of the wavelet packet energy (WPE) of vibration signals to identify the location and size of damage. They accurately located and measured minor damage in steel beams, proving robust to measurement noise with proper wavelet function and decomposition level selection, based on numerical and experimental results. This paper showed that varying wavelet functions affects the accuracy of damage localization. Jiang et al. [36] introduced a hybrid method for accurately detecting cracks in beam-like structures. By decomposing the beam's vibration mode shape using the wavelet transform and applying fractal dimension (FD) to the resulting signals, the method effectively identifies singularities indicative of cracks. This approach overcomes the limitations of traditional methods, enabling accurate detection of even small cracks in noisy environments. The Daubechies 4 (Db4) wavelet function was used to obtain the wavelet coefficients from the mode shape. Nigam et al. [37] presented a cost-effective, vibration-based method for crack localization in beam structures. Their proposed method utilized DWT to analyze slope discontinuities in beam deflection caused by the crack. A low-cost digital imaging technique measured beam deflection, employing algorithms to remove noise and optimize edge detection (e.g., Canny operator) for accurate signal input. Simulation and experimental results demonstrated the method's effectiveness in detecting cracks of varying depths, even under noisy conditions.

Researchers have employed CWT and DWT with various wavelet functions for damage detection in composite structures, and studies indicate that the choice of wavelet function influences detection accuracy. According to the literature [38–42], some wavelet functions are weak at detecting damage when using the wavelet transform. This research develops a novel and efficient family of Legendre wavelet functions for damage detection in laminated composite beams. Thus, the novelty of this research is to design a family of new wavelet functions called Legendre wavelet functions to have better performance in detecting damage in laminated composite beam structures than conventional wavelet functions.

2. Legendre wavelet functions

Wavelet functions can be defined numerically or analytically. While many numerical wavelets lack closed-form expressions, even analytical wavelets require sampling for numerical implementation in wavelet transforms. In this study, we develop the Legendre wavelet functions, which are numerical wavelet functions inspired by the exact formulation of Legendre functions. For this, even-degree Legendre polynomials are sampled at 10 equally spaced points to have a grid of Legendre polynomial values with ten sampling points. Then, the Legendre wavelet functions using numerical differentiations of some Legendre polynomials are designed.

As well-known Legendre polynomials are orthogonal functions that can be analytically defined as follows [43]:

$$P_n(x) = \frac{1}{2^n n!}\frac{d^n}{dx^n}\left(x^2-1\right)^n \tag{1}$$

a derivative recurrence relation for Legendre polynomials is expressed [44]:

$$\left(1-x^2\right)P_n^{'}(x) = n(P_{n-1}(x) - xP_n(x)) \tag{2}$$

Legendre wavelet functions are based on the first derivative of ten-sampled Legendre polynomials, subject to the condition that:

$$P_n^{'}(x) = \frac{n(P_{n-1}(x) - xP_n(x))}{(1-x^2)} \tag{3}$$

where $n = \{2k+1 | k \in \uparrow\mathbb{Z}, k \geq 1\}$. In other words, we can design the Legendre wavelet functions using $P_n^{'}(x)$ when $n \in \{3, 5, 7, 9, 11, 13, \ldots\}$.

On the other hand, for a function to be a wavelet function $\psi(\mathrm{x})$, the following two conditions must be met simultaneously.

Zero-mean condition, which means the mean of wavelet function $\psi(\mathrm{x})$ is zero [45]:

$$\int_{-\infty}^{+\infty} \psi(\mathrm{x})dx = 0 \tag{4}$$

and the finite energy condition for the wavelet functions [46]:

$$\int_{-\infty}^{+\infty} |\psi(\mathrm{x})|^2 dx < \infty \tag{5}$$

This means that the wavelet function $\psi(\mathrm{x})$ has to have a finite energy.

To numerically implement the Legendre polynomials on a discretized grid, we set $P_0(x) = 1$ and$P_1(x) = x$, and for other points, Bonnet's recursion formula is used as follows [47]:

$$P_n(x) = \frac{(2n-1)xP_{n-1}(x) - (n-1)P_{n-2}(x)}{n}, n \geq 2 \tag{6}$$

For approximating $P_n^{'}(x) = \frac{dP_n}{dx}$ on the grid, the finite difference method is used. By defining $\Delta x = h = x_1 - x_2$ as the step size, for the first point (left boundary), the forward difference formula is used as follows [48]:

$$P_n^{'}(x_1) \approx \frac{P_n(x_2) - P_n(x_1)}{h} \tag{7}$$

For the last point (right boundary), the backward difference formula is used as follows:

$$P_n^{'}(x_{end}) \approx \frac{P_n(x_{end}) - P_n(x_{end-1})}{h} \tag{8}$$

For the interior points, the central difference formula is used as follows:

$$P_n^{'}(x_{end}) \approx \frac{P_n(x_{i+1}) - P_n(x_{i-1})}{2h} \tag{9}$$

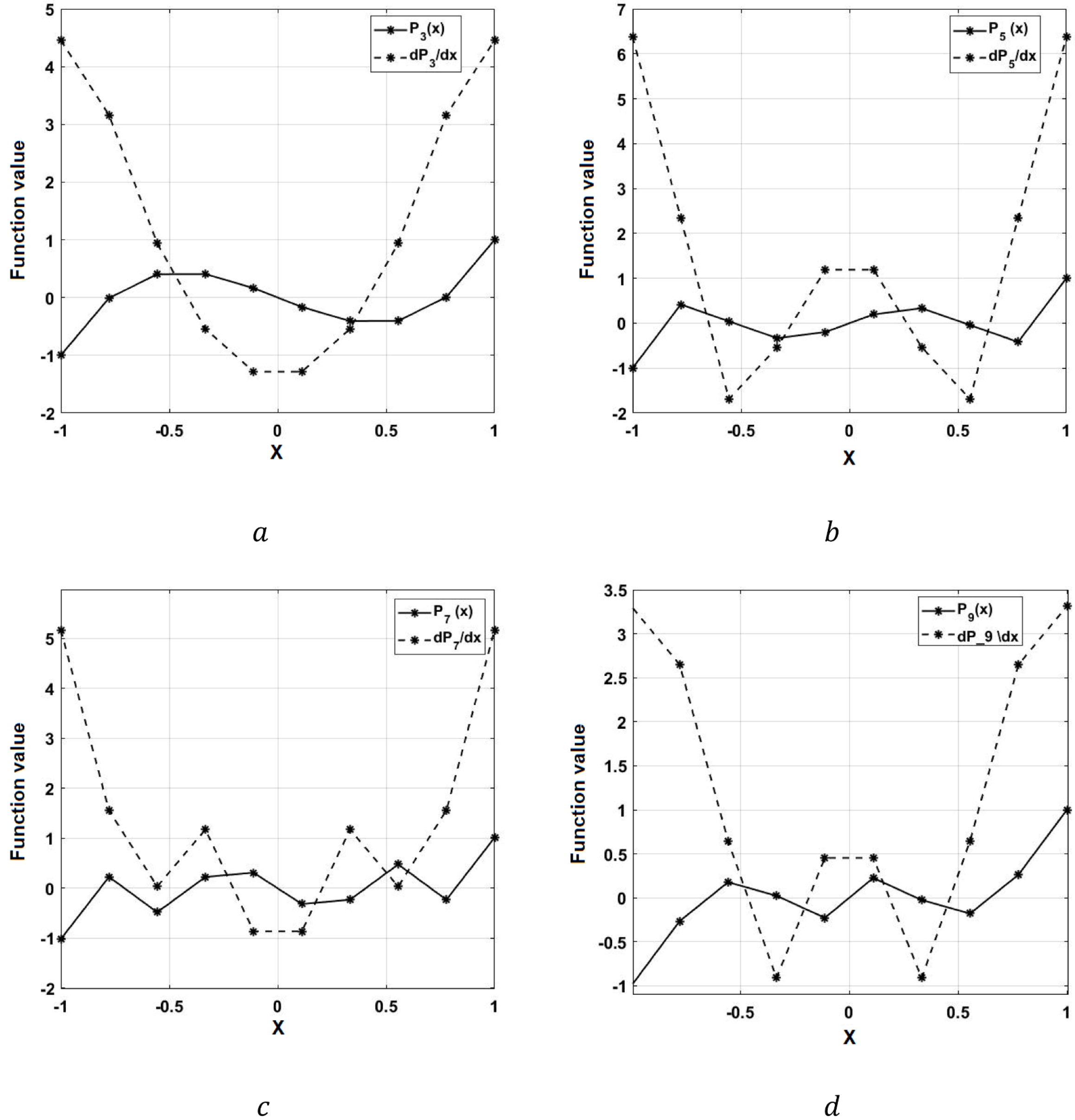

Fig. 1. The first-order numerical differentiation of Legendre functions on a grid containing ten sampling points: *a*) the third-degree Legendre function sampled at 10 points ($P_3(x)$) and its numerical derivative ($\frac{dP_3}{dx}$), *b*) the fifth-degree Legendre function sampled at 10 points ($P_5(x)$) and its numerical derivative ($\frac{dP_5}{dx}$), *c*) the seventh-degree Legendre function sampled at 10 points ($P_7(x)$) and its numerical derivative ($\frac{dP_7}{dx}$), and), *c*) the ninth-degree Legendre function sampled at 10 points ($P_9(x)$) and its numerical derivative ($\frac{dP_9}{dx}$).

Fig. 1 shows plots of P_n sampled at 10 equally spaced points in the interval $[-1\ 1]$ for $n \in \{3,5,7,9\}$ and their corresponding numerical derivatives. Table A1 (presented in Appendix A) indicates the values of $\frac{dP_n}{dx}$ when $n \in \{3,5,7,9,11,13,15,17\}$.

Functions can be wavelet functions that satisfy both the zero-mean and finite energy conditions. $\frac{dP_n}{dx}$ when $n \in \{3,5,7,9,11,13,\ldots\}$ satisfies the finite energy condition, but according to Table A1, when the Legendre polynomials exist in a grid containing ten sampling points, they do not have zero mean. Therefore, the zero-mean condition is not satisfied for them. However, according to Tables A2 (presented in Appendix A), Legendre wavelet functions are derived using the forward difference of q-order derivative from the numerical vectors presented in Table A1, if and only if $q = 3,5,7$ to have Legendre wavelet functions with seven, five, three sampling points, respectively.

Fig. 2 shows the Legendre wavelet functions from third degree to ninth degree.

Fig. 3 indicates the Legendre wavelet functions from eleventh degree to seventeenth degree.

Because ψ_3 to ψ_{17} with sampling points 3,5,7, and 9 have the zero mean. To reduce edge effects in the wavelet transform, also two other versions of the Legendre wavelet functions are presented with three and five sampling points (Table A3).

Thus, in this study, in order to design Legendre wavelet functions, first, the Legendre polynomials P_n sampled at 10 equally spaced points in the interval $[-1\ 1]$ when $n \in \{3,5,7,9,11,13,15,17\}$ and their corresponding numerical derivative $\frac{dP_n}{dx}$ when $n \in \{3,5,7,9,11,13,15,17\}$ were calculated. Then, the forward difference of q-order derivative, if and only if $q = 3,5,7$, is applied to $\frac{dP_n}{dx}$ to obtain Legendre wavelet functions with seven, five, three sampling points, respectively.

By denoting Legendre wavelet functions as ψ_L, the wavelet transform is defined as follows:

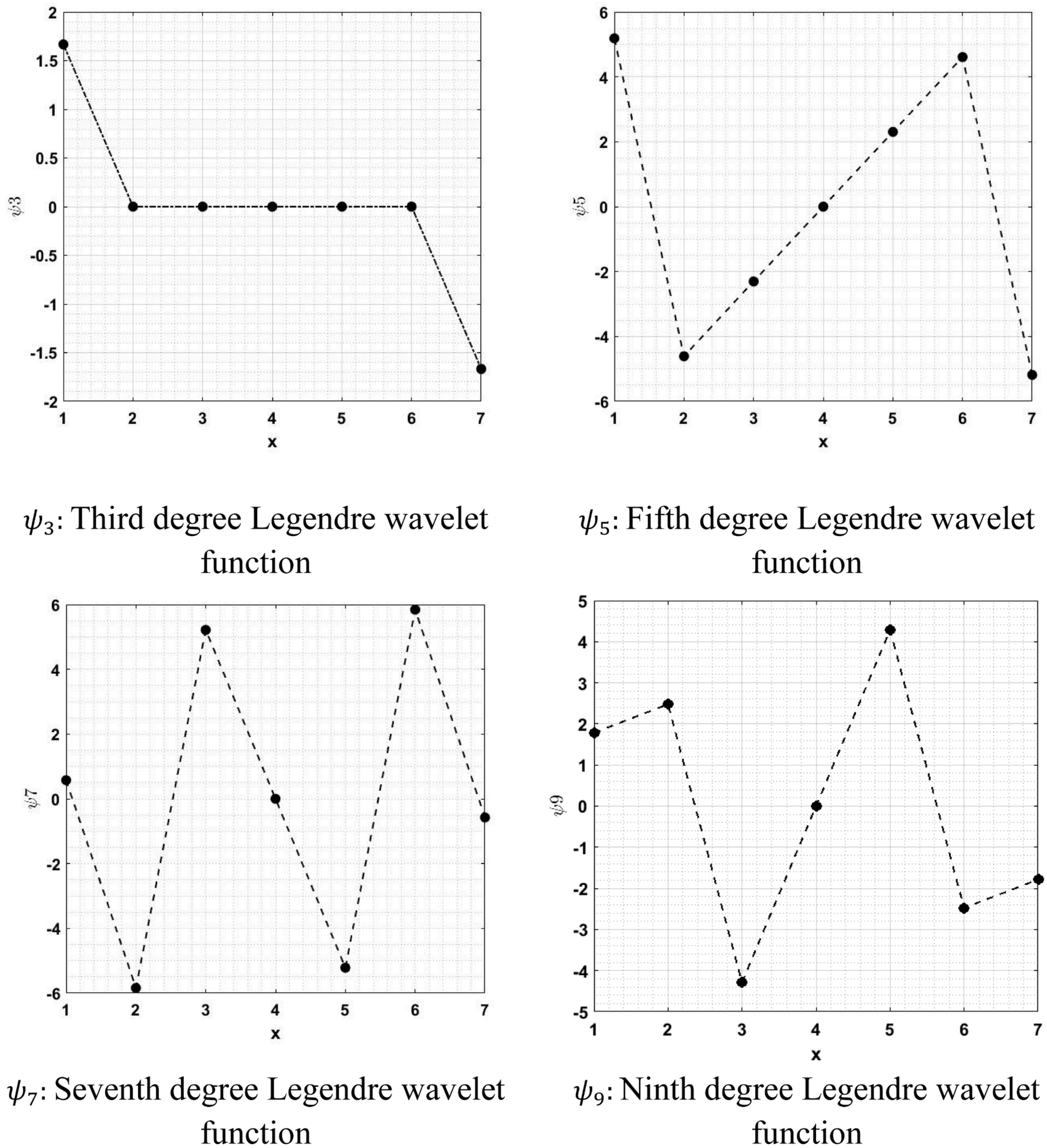

Fig. 2. Legendre wavelet functions from the third degree to the ninth degree.

$$WT = \frac{1}{\sqrt{s_0}} \int_{-\infty}^{+\infty} f(x)\psi_L\left(\frac{x-u}{s_0}\right)dx \tag{10}$$

where $f(x)$ is the original signal, u is shifting parameter, and s_0 is a given scaling parameter. In this study, we set $s_0 = 1$.

3. Methodology

This study uses a semi-analytical, closed-form solution derived from the governing differential equation for simply supported boundary conditions. The material is modeled using classical lamination theory (CLT) to calculate effective bending stiffness (D_{11}) and mass properties. Classical beam theory (CBT), also known as Euler-Bernoulli beam theory, is employed, neglecting transverse shear deformation and rotary inertia by assuming plane cross-sections remain plane and perpendicular to the neutral axis after bending. For the solution method, the analytical closed-form solution is used. The paper utilizes the known analytical solution for the natural frequencies of a simply supported (SS) Euler-Bernoulli beam, modified to incorporate the composite stiffness (D_{11}) and mass ($\overline{m}$) determined by CLT. The CLT relates the resultant forces (N) and moments (M) to the mid-plane strains (ε_0) and curvatures (κ) through the ABD matrix:

$$\begin{pmatrix} N_x \\ N_y \\ N_{xy} \\ M_x \\ M_y \\ M_{xy} \end{pmatrix} = \begin{pmatrix} [A] & [B] \\ [B] & [D] \end{pmatrix} \begin{pmatrix} \varepsilon_{x0} \\ \varepsilon_{y0} \\ \gamma_{xy0} \\ \kappa_x \\ \kappa_y \\ \kappa_{xy} \end{pmatrix} \tag{11}$$

where [A] is the Extensional Stiffness Matrix. [B] is the Coupling Stiff-

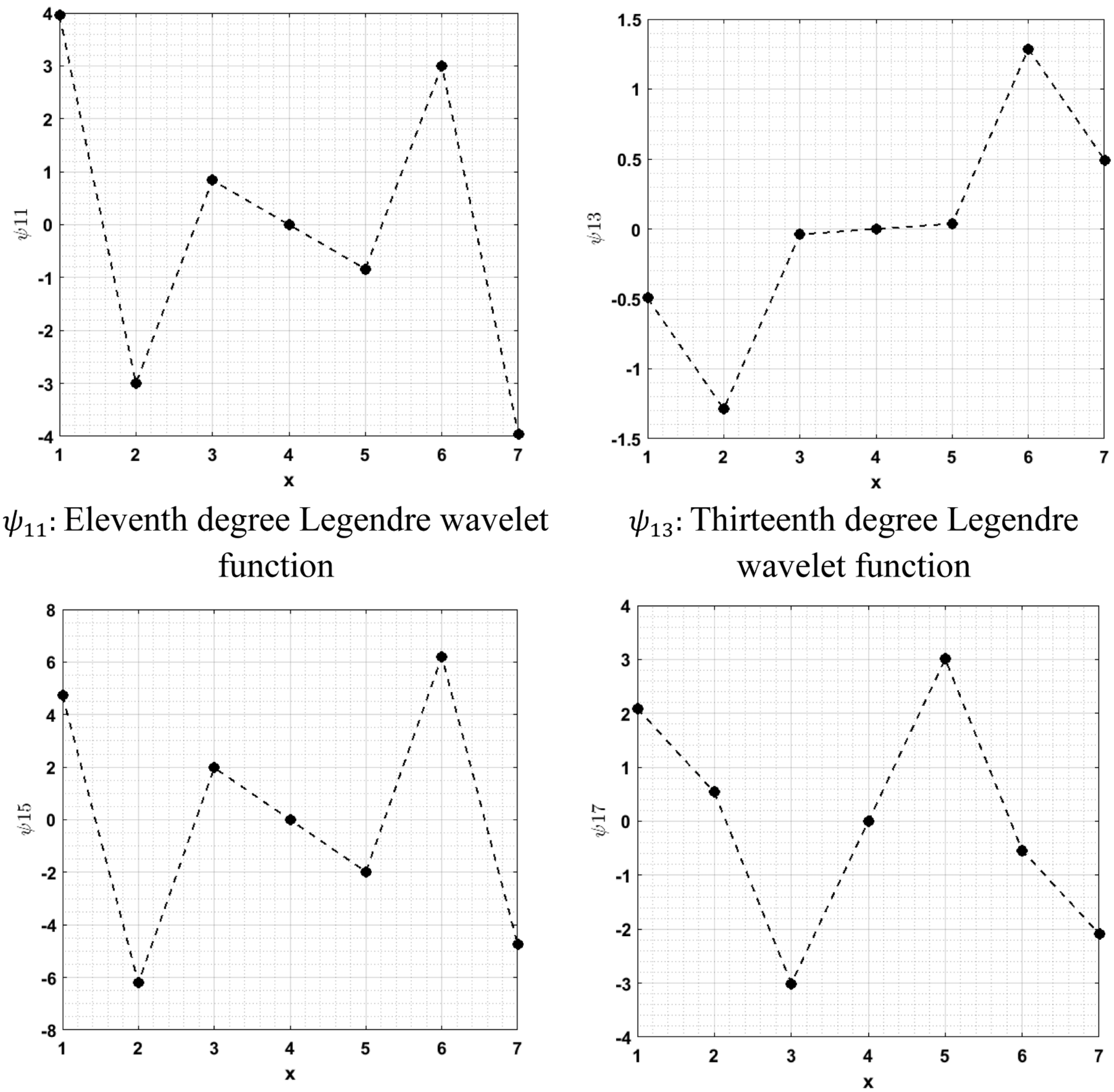

ψ_{11}: Eleventh degree Legendre wavelet function

ψ_{13}: Thirteenth degree Legendre wavelet function

ψ_{15}: Fifteenth degree Legendre wavelet function

ψ_{17}: Seventeenth degree Legendre wavelet function

Fig. 3. Legendre wavelet functions from eleventh degree to seventeenth degree.

Table 1
Material properties of the considered laminated composite beam considered in this study [49].

No.	Property	Symbol	Value	descriptions
2	Longitudinal Young's Modulus	E_1	139 GPa	Stiffness along the fiber direction.
3	Transverse Young's Modulus	E_2	8 GPa	Stiffness perpendicular to the fiber direction.
4	Shear Modulus	G_{12}	5 GPa	Shear stiffness in the 1–2 plane.
5	Major Poisson's Ratio	ν_{12}	0.3	Transverse strain in the 2-direction due to strain in the 1-direction
6	Density	ρ	1760 kg/m3	Mass density of the composite material.

Table 2
Five damage scenarios considered in numerical investigations.

Scenario No.	Location of damage	Level of damage
1	40	0.5 %
2	20	0.1 %
3	70	0.2 %
4	60	0.15 %
5	90	0.1 %

ness Matrix (linking extension to bending). [D] is the Bending Stiffness Matrix. The elements of these matrices are calculated by summing the contribution of each ply (k):

$$[A] = \sum_{k=1}^{N} [\overline{Q}]_k (z_k - z_{k-1}) \tag{12}$$

$$[B] = \frac{1}{2} \sum_{k=1}^{N} [\overline{Q}]_k \left({z_k}^2 - {z_{k-1}}^2\right) \tag{13}$$

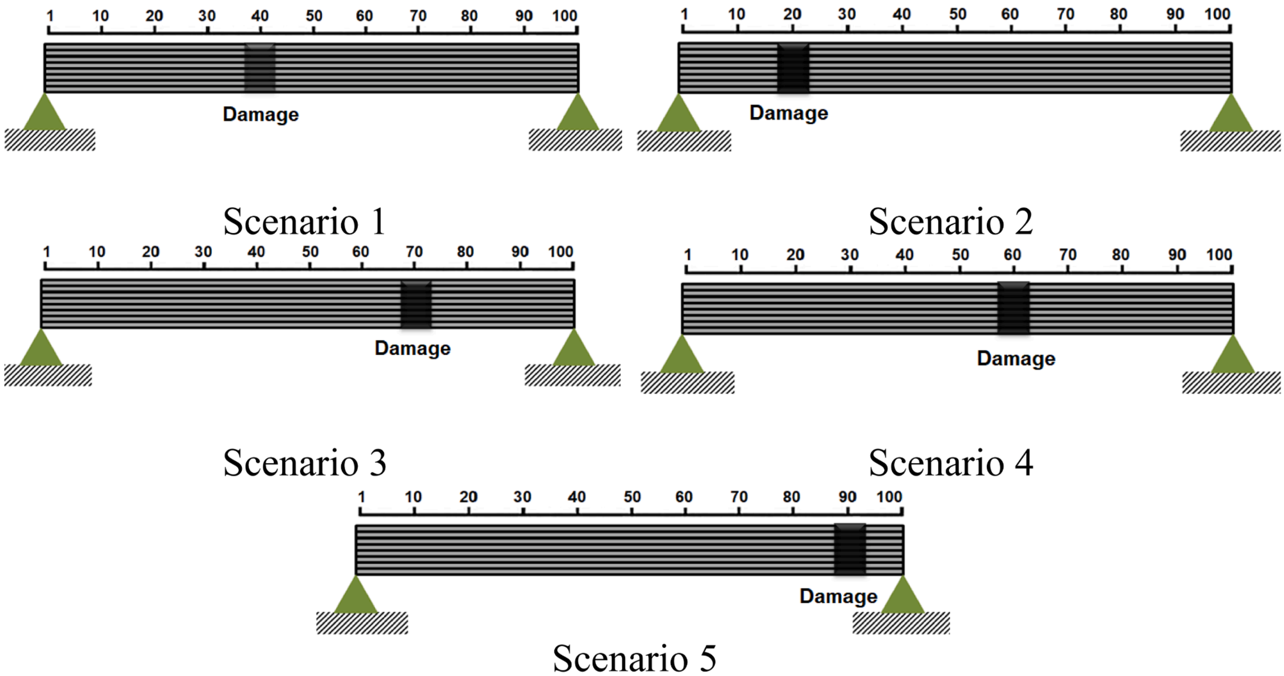

Fig. 4. Graphical representation of damage scenarios presented in Table 2.

$$[D] = \frac{1}{3}\sum_{k=1}^{N}[\overline{Q}]_k\left({z_k}^3 - {z_{k-1}}^3\right) \tag{14}$$

where $[\overline{Q}]_k$ is the transformed reduced stiffness matrix for the k^{th} ply, and z_k and z_{k-1} are the z-coordinates of the top and bottom surfaces of the ply, respectively. For an effective bending stiffness (D_{11}), this study assumes pure bending vibration along the beam axis (x-direction) and uses the D_{11} term from the [D] matrix, while neglecting the coupling matrix [B] (meaning $\varepsilon_0 = 0$).

$$M_x = D_{11}\kappa_x = -D_{11}\frac{\partial^2 w}{\partial x^2} \tag{15}$$

The value D_{11} is:

$$D_{11} = D(1,1) \tag{16}$$

The mass of the beam per unit length ($\overline{m}$) is calculated simply as:

$$\overline{m} = \rho.b.h \tag{17}$$

where ρ is the density, b is the width, and h is the total thickness. The equation of motion for the free vibration of a beam based on the Euler-Bernoulli assumption, incorporating the composite stiffness D_{11} and mass $\overline{m}$, is:

$$D_{11}\frac{\partial^4 w(x,t)}{\partial x^4} + \overline{m}\frac{\partial^2 w(x,t)}{\partial t^2} = 0 \tag{18}$$

where $w(x,t)$ is the transverse deflection of the beam. By assuming a harmonic solution $w(x,t) = W(x)cos(\omega t)$, the spatial part of the equation becomes the Eigenvalue problem:

$$D_{11}\frac{\partial^4 W(x)}{\partial x^4} - \overline{m}\omega^2 W(x) = 0 \tag{19}$$

For a Simply Supported (SS) beam, the boundary conditions are zero deflection and zero moment at both ends:

$$W(0) = 0, W''(0) = 0 \tag{20}$$

$$W(L) = 0, W''(L) = 0 \tag{21}$$

The closed-form solution for the mode shapes $W_n(x)$ is sinusoidal, and the wave number λ_n is:

$$W_n(x) = C_n \sin\left(\frac{n\pi x}{L}\right) \tag{22}$$

$$\lambda_n = \frac{n\pi}{L}, n = 1, 2, 3, \ldots \tag{23}$$

Note that for damage detection, this study considers only flexural modes. The natural angular frequency (ω_n) is directly derived from the eigenvalue problem using λ_n:

$$\omega_n = {\lambda_n}^2\sqrt{\frac{D_{11}}{\overline{m}}} \tag{24}$$

$$\omega_n = \left(\frac{n\pi}{L}\right)^2\sqrt{\frac{D_{11}}{\overline{m}}}\left[\frac{rad}{s}\right] \tag{25}$$

The final natural frequency (f_n) in Hertz (Hz) used is as follows:

$$f_n = \frac{\omega_n}{2\pi} = \frac{1}{2\pi}\left(\frac{n\pi}{L}\right)^2\sqrt{\frac{D_{11}}{\overline{m}}}[Hz] \tag{26}$$

Thus, the wavelet transform expression based on the proposed method is stated as follows:

$$WT = \frac{1}{\sqrt{s_0}}\int_{-\infty}^{+\infty} W_n(x)\psi_L\left(\frac{x-u}{s_0}\right)dx \tag{27}$$

4. Results

4.1. 1 Numerical investigation

Numerical simulations for free vibration of the carbon-epoxy laminated composite beam are performed based on the procedure presented in [32] for the analysis of vibration mode shapes. A MATLAB code is established to calculate the free vibration of a simply supported laminated composite beam, using The Classical Beam Theory (CBT). CBT determines the effective bending stiffness (D_{eff} or D_{11}) by: first, calculating each ply's reduced stiffness matrix (Q_{local}) from its material

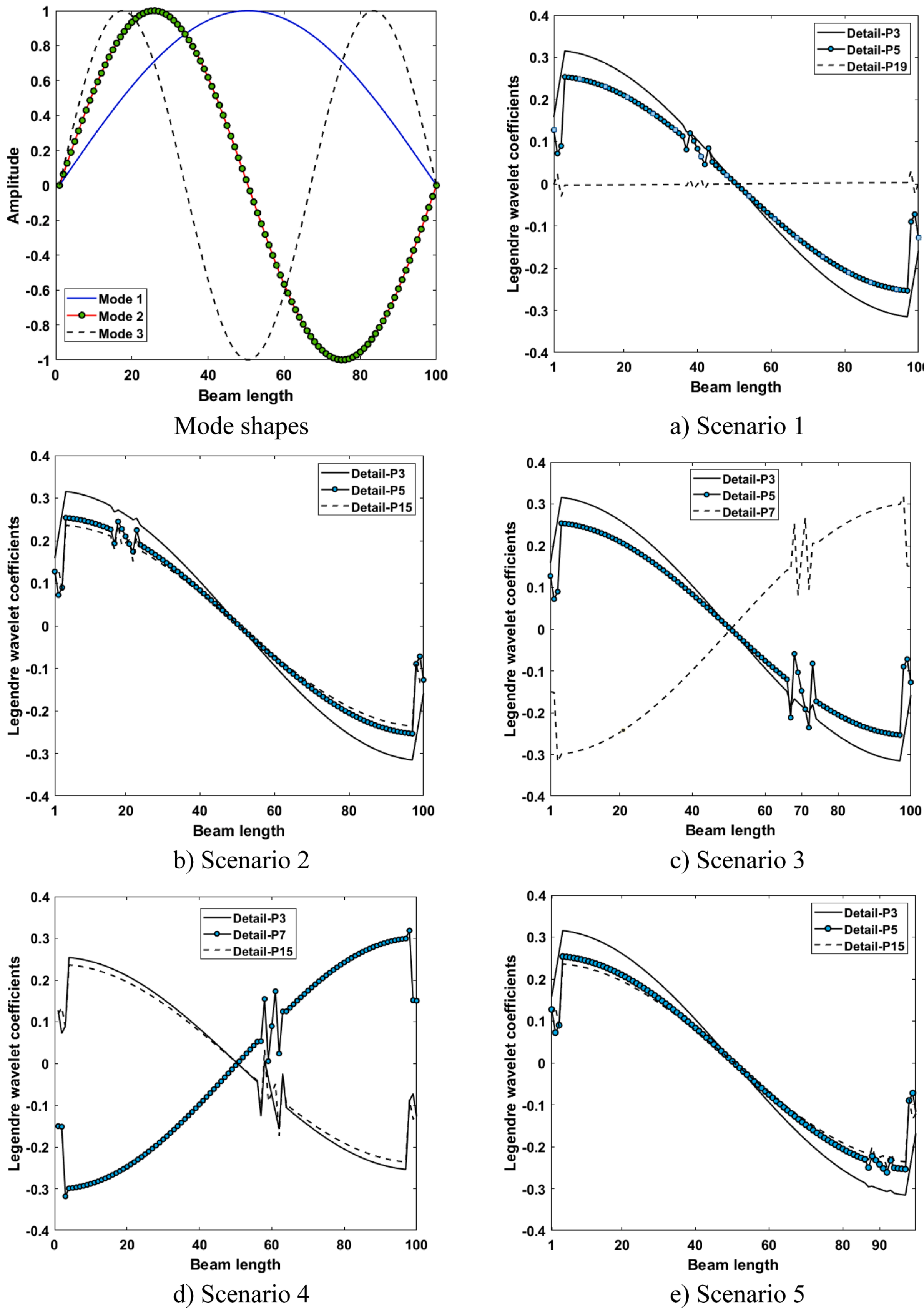

Fig. 5. Numerical mode shapes and results of damage scenarios using the wavelet transform with the proposed Legendre wavelet functions.

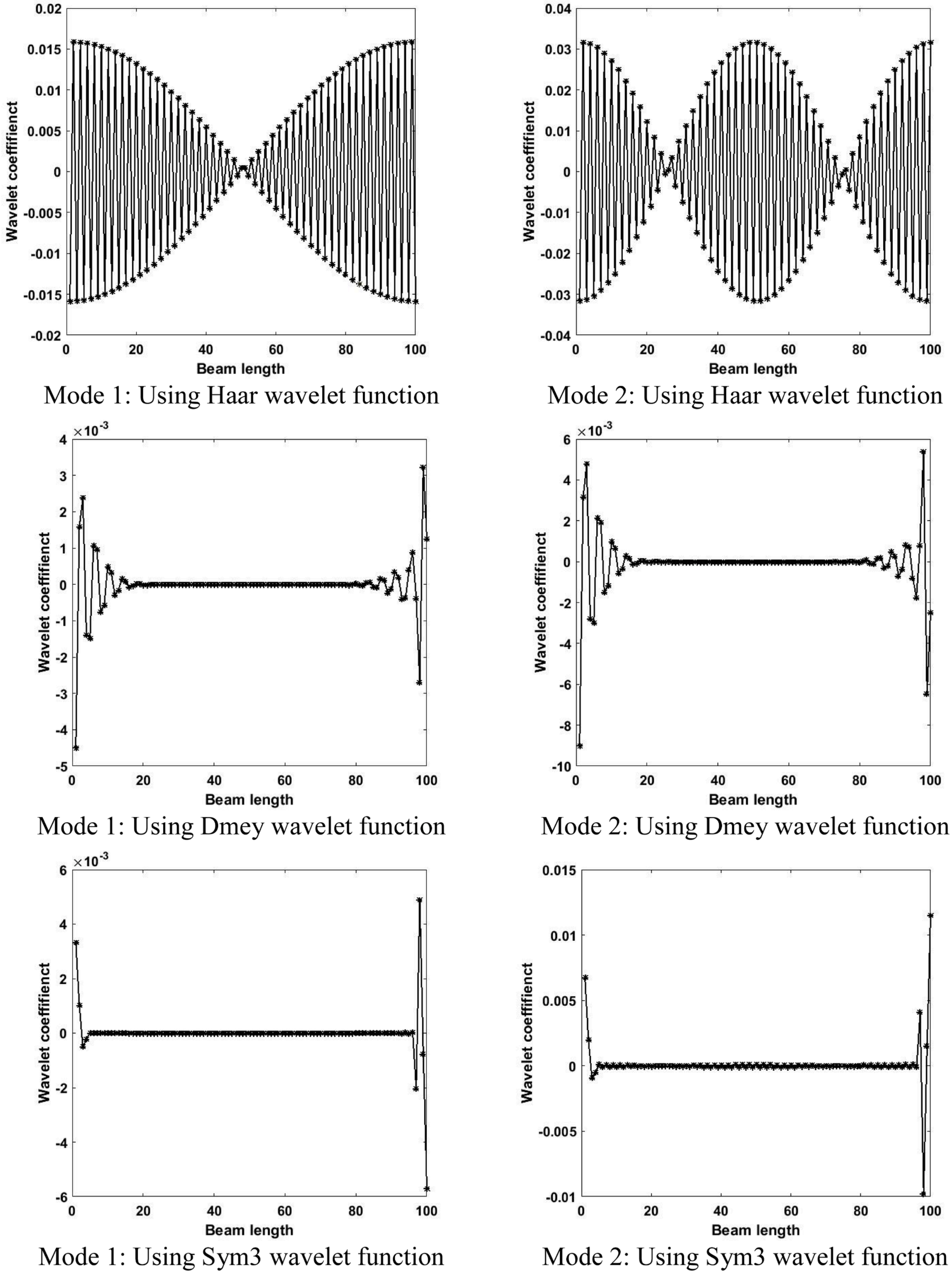

Fig. 6. Numerical results of damage scenarios using the wavelet transform with the conventional wavelet functions.

properties (E_1, E_2, ν_{12}, G_{12}); then, transforming Q_{local}) into the global stiffness matrix ($\overline{Q}$) based on ply orientation (θ_k). The D matrix is then computed by summing each ply's contribution of $\overline{Q}^k$) multiplied by the integral of $\frac{z^2}{2}$ across its thickness ($z_k^3 - z_{k-1}^3$). Euler-Bernoulli Beam Theory is use to determine mode shapes of a simply supported laminated composite beam by solving a characteristic equation. The mode shape $W_n(x)$ is given by the sinusoidal function $W_n(x) = \sin\left(\frac{n\pi x}{L}\right)$. The beam is 0.1 m long (L) and 0.05 m wide (b). The composite consists of plies with a single ply thickness (t_{ply}) of 0.125×10^{-3} m. We consider an eight-ply laminate with a stacking sequence (θ) of [0°, 90°, 0°, 90°, 0°, 90°, 0°, 90°] results in a total laminate thickness (h) of 1×10^{-3} m. Table 1 shows the material properties of the considered laminated composite beam considered in this study.

Fig. 7. Experimental modal analysis setup used in the current study location of damage in the considered laminated composite beam.

Five numerical damage scenarios, detailed in Table 2 and Fig. 4, assess the performance and robustness of the Legendre wavelet transform for damage detection in laminated composite beams, with damage locations and levels (mostly under 0.2 %) varying across scenarios. To apply damage to the model, we increase the percentage of the deviation from the sampling point in the mode shape corresponding to each scenario. For example, in the first scenario, the amplitude of the mode shape at sampling point 40 is increased by 0.5 %.

Fig. 4 indicates the graphical representation of damage scenarios presented in Table 2.

Fig. 5 shows numerical mode shapes and results of damage scenarios using the wavelet transform with the proposed Legendre wavelet function. We use the first mode shapes as fundamental mode shapes for damage detection. The Legendre wavelet function with seven sampling points is used for these scenarios.

Also, the Legendre wavelet function with five or three sampling points are developed in this study. However, the results presented in Fig. 5 show that the proposed wavelet function is efficient for damage detection in all considered scenarios. By comparing Table 2 and Fig. 4 with the results presented in Fig. 5, we find that in scenario 1 (Fig. 5a), the Legendre wavelet function constructed using the Legendre polynomial of degree 5 (P5) is the most effective wavelet function for damage detection. Fig. 5b shows the damage detection results of scenario 2. According to this figure, with the increase of the degree of the Legendre wavelet function, the accuracy of damage detection increases, and at the same time, edge effects also decrease. In this scenario, Legendre wavelet functions constructed using Legendre polynomials of degrees five and fifteen (i.e., P5 and P15) yield better results than the Legendre wavelet function of degree 3 (P3). Fig. 5c indicates the results of damage detection for scenario 3. Findings show that for this scenario, all of the Legendre wavelet functions (those constructed using polynomials of degrees 3, 5, 7 (P3, P5, and P7) can detect damage with high accuracy. Fig. 5d shows the results of damage detection for scenario 4. Results indicate that for this scenario, all of the Legendre wavelet functions (i.e., those created based on polynomials of degrees 3, 7, and 15 (P3, P7, and P15) can detect damage with high accuracy, like in the previous scenario. Fig. 5e denotes the results of damage detection for scenario 5. Results indicate that Legendre wavelet functions constructed using Legendre polynomials of degrees five and fifteen (i.e., P5 and P15) yield better results than the Legendre wavelet function of degree 3 (P3).

Fig. 5 shows that damage detection using Legendre wavelet functions is most effective when the damage is located in the middle of the beam. Detection becomes more challenging as the damage approaches the beam's ends. The correlation with Legendre wavelet functions is affected by the mode shape's steeper slopes at the beam's center compared to its boundaries. In general, findings indicate that as the degree of the Legendre wavelet function increases, the accuracy of damage detection increases. Edge effects are inherent in wavelet transforms due to incomplete convolution. However, Legendre wavelet functions mitigate this issue; increasing the degree of the Legendre wavelet function reduces the number of wavelet coefficients affected by edge effects. This, along with their exact expression and ease of implementation, distinguishes Legendre wavelet functions from other numerical wavelet functions.

Fig. 5 indicates that scenario 5 is the most challenging damage detection case. This scenario was successfully detected using the proposed wavelet transform based on Legendre functions. Consequently, Fig. 6 presents results for scenario 5 using wavelet functions, allowing for a comparison between the proposed methodology and the conventional wavelet transform. In Fig. 6, the first and second mode shapes of scenario five were processed using three types of wavelet functions, namely Haar, Dmey, and Sym3. The Haar wavelet transform fails to detect damage in the first two mode shapes. Dmey wavelet functions introduce edge effects that reduce damage detection accuracy. The Sym3 wavelet function, when used with the first mode shape, also fails to detect damage. While the Sym3 wavelet function can detect damage location using the second mode shape, it suffers from significant edge effects. These results demonstrate the effectiveness of Legendre wavelet-based transforms for structural damage detection, as proposed in this paper.

4.2. 2 Experimental investigation

Experimental modal analysis is performed on a 60 cm long carbon-epoxy laminate beam with a crack at 25 cm along the beam length to validate the proposed methodology for practical engineering applications. The beam (Fig. 7) consists of four carbon fiber layers oriented at $[90^{\circ}/0^{\circ}/90^{\circ}0^{\circ}]$. The experimental setup uses a TIRA-TV5220 vibration shaker, an 8200BK force gauge having a 2647A amplifier, and a Laser Doppler vh300 laser vibration meter connected to a 3560D analyzer.

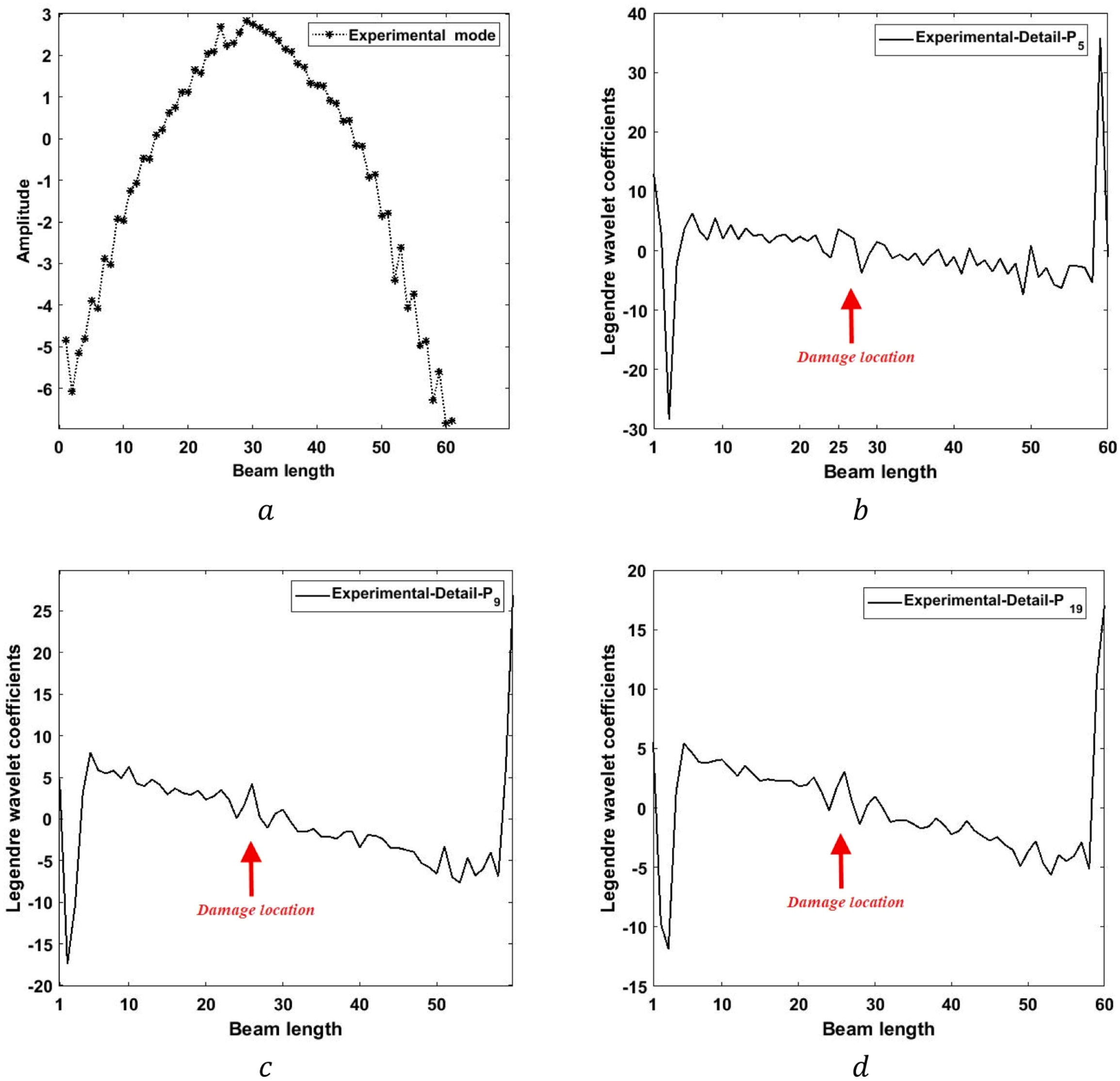

Fig. 8. Experimental mode shape and results of damage scenarios using the wavelet transform with the proposed Legendre wavelet functions.

Suspended by soft elastics, the beam's velocity response is measured at 60 points using the laser vibrometer, while the shaker applies force at point 45. The analyzer processes the vibrometer and force gauge signals to determine Frequency Response Functions (or FRFs), from which experimental mode shapes are extracted.

Free-free boundary conditions are applied in the experimental modal analysis. Literature indicates that a change in boundary conditions does not compromise the accuracy of damage detection via wavelet transform, as this method is sensitive to abrupt, localized mode shape variations. Furthermore, free-free boundary conditions, easily implemented in the lab, minimize extraneous effects on result accuracy. Therefore, we employed free-free conditions to acquire the experimental mode shape.

Fig. 8 presents the first experimental mode shape and damage detection results using the fifth, ninth, and nineteenth Legendre wavelet functions. Consistent with numerical findings, damage detection accuracy improves with increasing Legendre wavelet degree and with a higher number of mode shape sampling points. The proposed Legendre wavelet method effectively detects damage in the laminated composite beam with acceptable accuracy, even with only 60 sampling points, particularly when employing higher-degree Legendre wavelets.

Note that Laboratory damage identification is more challenging than with numerical data due to fewer sampling points and signal noise, limitations arising from signal acquisition rather than the processing method itself.

4.3. Discussion

In this study, we design a new family of wavelet functions called Legendre wavelet functions to detect damage in laminated composite beam structures. Based on numerical findings, the designed Legendre wavelet functions can detect damage in all numerical damage scenarios. In other words, damages in different locations with different level or severity can accurately be detected when we use Legendre wavelet functions in the wavelet transform. Furthermore, the experimental investigations are considered to evaluate the performance of the Legendre wavelet functions for the practical damage detection. In the numerical damage scenarios, there are 100 sampling points, but in the experimental damage scenario, there are 60 sampling points.

It is obvious and significant that the fewer the number of sampling points, the less smooth the signal and the more difficult and inaccurate the damage detection using the wavelet transform becomes. However, in the experimental results with fewer sampling points, the damage detection was performed with high accuracy. A major reason for such success is that the Legendre wavelet functions at a low number of samples (such as seven, five, and three sampling points) have sharp wavelets with steep slopes. This geometric feature in the Legendre wavelet functions designed in this research enables the wavelet transform to detect local subtle jumps in smooth signals with many sampling points. Therefore, such functions can be very promising for detecting signal singularities.

According to the findings of this research, it is difficult to detect damage near the boundaries using wavelet transform. This is due to the incomplete convolutional nature of the wavelet transform at the edges. Also, on the other hand, the boundary conditions introduce perturbations in the measured signals that can manifest as false damage indications close to the supports (e.g., locations 98 or 99). This effect poses a challenge for accurately detecting and localizing damage that occurs very close to the supports. We acknowledge this challenge and suggest it for future works aimed at improving damage detection accuracy near supports.

5. Conclusions

This research develops a new type of wavelet function, called the Legendre wavelet function, for structural damage identification in laminated composite beams. We assessed the proposed performance of the Legendre-based wavelet transform through numerical and experimental validation. Legendre wavelet functions are developed based on differentiating the first derivative of the explicit Legendre polynomial relations. On a ten-digit grid, Legendre wavelet functions with three types of sampling numbers (i.e., Legendre functions with seven sampling points, five plot points, and three plot points) are developed. Different damage scenarios are considered to evaluate the performance of these functions in the wavelet transform. Numerical and experimental results demonstrate the effectiveness of the proposed methodology for damage identification in laminated composite beams. The proposed method offers implementation simplicity and improves damage identification accuracy with a higher degree of Legendre wavelet function.

5.1. Suggestions for future studies

According to the findings of this research, it is difficult to detect damage near the boundaries using the wavelet transform. This is due to the incomplete convolutional nature of the wavelet transform at the edges. Also, on the other hand, the boundary conditions introduce perturbations in the measured signals that can manifest as false damage indications close to the supports (e.g., locations 98 or 99). This effect poses a challenge for accurately detecting and localizing damage that occurs very close to the supports. We acknowledge this challenge and suggest it for future works aimed at improving damage detection accuracy near supports.

Furthermore, according to the findings of this study, it is evident that the Legendre wavelet functions can detect subtle local variations in one-dimensional signals with a high number of smooth sampling points. Future studies should extend these one-dimensional functions to two-dimensional Legendre functions to explore their potential for detecting local singularities in two-dimensional signals for damage detection in composite structures like laminated plates.

CRediT authorship contribution statement

Morteza Saadatmorad: Writing – original draft, Visualization, Validation, Software, Methodology, Formal analysis, Data curation, Conceptualization. **Nicholas Fantuzzi:** Writing – review & editing, Visualization, Supervision, Software, Resources, Project administration. **Pietro Russo:** Writing – review & editing, Visualization, Project administration, Funding acquisition.

Declaration of competing interest

The authors declare that they have no known competing financial interests or personal relationships that could have appeared to influence the work reported in this paper.

Acknowledgments

The publication was made with funding from the Ministry of University and Research (MUR) under the FIS 2 Grant, Project TOSSTO, no. FIS-2023-01465, (CUP: J53C25000610001), project PRIN 2020, no. 2020F23HZ7_003 (CUP: J35F22000640001) and PRIN 2022, no. 2022YLNJRY (CUP: J53D23002500006) funded by the European Union – Next Generation EU.

Appendix A

Table A1
The values of the first four derivative Legendre functions on a grid with ten sampling points.

4.45679	3.160494	0.938272	−0.54321	−1.28395	$\frac{dP_3}{dx}$	−1.28395	−0.54321	0.938272	3.160494	4.45679
6.377229	2.344307	−1.68861	−0.53635	1.192044	$\frac{dP_5}{dx}$	1.192044	−0.53635	−1.68861	2.344307	6.377229
5.173122	1.560918	0.036896	1.176831	−0.86121	$\frac{dP_7}{dx}$	−0.86121	1.176831	0.036896	1.560918	5.173122
3.312788	2.650591	0.648362	−0.90969	0.454348	$\frac{dP_9}{dx}$	0.454348	−0.90969	0.648362	2.650591	3.312788
3.509874	2.527073	0.115586	0.231672	−0.12927	$\frac{dP_{11}}{dx}$	−0.12927	0.231672	0.115586	2.527073	3.509874
5.117095	1.717329	0.190765	0.043806	−0.01045	$\frac{dP_{13}}{dx}$	−0.01045	0.043806	0.190765	1.717329	5.117095
5.593069	2.392668	−0.94482	0.309076	−0.05346	$\frac{dP_{15}}{dx}$	−0.05346	0.309076	−0.94482	2.392668	5.593069
4.387112	2.615019	0.201099	−0.76495	0.255278	$\frac{dP_{17}}{dx}$	0.255278	−0.76495	0.201099	2.615019	4.387112

Table A2
Legendre wavelet functions with seven sampling points (ψ_3 to ψ_{17}).

			ψ_3:				mean
1.666667	-4.44×10^{-16}	1.55×10^{15}	-6.66×10^{16}	-1.55×10^{-15}	2.89×10^{-15}	−1.66667	0
			ψ_5:				
5.185185	−4.60905	−2.30453	0	2.304527	4.609053	−5.18519	0
			ψ_7:				
0.575776	−5.84193	5.216007	1.33×10^{-15}	−5.21601	5.841928	−0.57578	≈0.0
			ψ_9:				
1.784206	2.477925	−4.28614	-1.78×10^{-15}	4.286141	−2.47793	−1.78421	≈0.0
			ψ_{11}:				
3.956259	−3.0046	0.837964	1.67×10^{-15}	−0.83796	3.004598	−3.95626	≈0.0
			ψ_{13}:				
−0.4936	−1.2869	−0.03845	-3.75×10^{-16}	0.038451	1.2869	0.493597	≈0.0
			ψ_{15}:				
4.728475	−6.20782	1.978966	-1.17×10^{-15}	−1.97897	6.207818	−4.72848	0
			ψ_{17}:				
2.089697	0.538408	−3.00651	2.22×10^{-15}	3.006508	−0.53841	−2.0897	≈0.0

Table A3
Legendre wavelet functions with three and five sampling points (ψ_3 to ψ_{17}).

			ψ_3:		
1.666667	-1.55×10^{-15}	−1.66667		Mean: -5.1810×10^{-16}	
1.666667	-4.22×10^{-15}	1.33×10^{-15}	5.33×10^{-15}	−1.66667	Mean: -8.4377×10^{-16}
			ψ_5:		
12.09877	0	−12.0988		Mean: 0	
12.09877	1.78×10^{-15}	0	-1.78×10^{-15}	−12.0988	Mean: 0
			ψ_7:		
50.02352	7.11×10^{-15}	−50.0235		Mean: 2.3685×10^{-15}	
17.47564	−16.2739	-3.55×10^{-15}	16.27394	−17.4756	Mean: 7.1054×10^{-16}
			ψ_9:		
−29.5582	-1.78×10^{-14}	29.5582		Mean: 3.5527×10^{-15}	
−7.45779	11.05021	5.33×10^{-15}	−11.0502	7.457786	Mean: −7.1054e-16
			ψ_{11}:		
20.16447	1.95×10^{-14}	−20.1645		Mean: -4.7370×10^{-15}	
10.80342	−4.68053	-5.55×10^{-15}	4.680526	−10.8034	Mean: -1.0658×10^{-15}
ψ_{13}:					
4.461751	2.00×10^{-15}	−4.46175		Mean: -3.2567×10^{-15}	
2.041753	−1.21	3.05×10^{-16}	1.209999	−2.04175	Mean: −8.8818e-16
			ψ_{15}:		
39.45458	-1.42×10^{-14}	−39.4546		Mean: 4.7370×10^{-15}	
19.12308	−10.1658	4.00×10^{-15}	10.16575	−19.1231	Mean: -1.4000×10^{-15}
			ψ_{17}:		
−15.0965	1.07×10^{-14}	15.09648		Mean: 4.7370×10^{-15}	
−1.99363	6.551424	-5.33×10^{-15}	−6.55142	1.993627	Mean: 2.1316×10^{-15}

Data availability

Data will be made available on request.

References

[1] M. Zanetti, D. Negri, D. Vandepitte, V. Tita, R. de Medeiros, Analyzing the influence of delamination on composite structures using modal analysis and statistical indices, Compos. Struct. (2025) 119427.
[2] V.G. De Menezes, G.S. Souza, D. Vandepitte, V. Tita, R. De Medeiros, Defect and damage detection in filament wound carbon composite cylinders: a new numerical-experimental methodology based on vibrational analyses, Compos. Struct. 276 (2021) 114548.
[3] D. Marques, F.R. Flor, R.D. Medeiros, C.D.C. Pagani Junior, V. Tita, Structural health monitoring of sandwich structures based on dynamic analysis, Lat. Am. J. Solids Struct. 15 (2018) e58.
[4] R. De Medeiros, D. Vandepitte, V. Tita, Structural health monitoring for impact damaged composite: a new methodology based on a combination of techniques, Struct. Health Monit. 17 (2) (2018) 185–200.
[5] F.I. Sakiyama, G.S. Veríssimo, F. Lehmann, H. Garrecht, Quantifying the extent of local damage of a 60-year-old prestressed concrete bridge: a hybrid SHM approach, Struct. Health Monit. 22 (1) (2023) 496–517.
[6] W. Fan, P. Qiao, Vibration-based damage identification methods: a review and comparative study, Struct. Health Monit. 10 (1) (2011) 83–111.
[7] D.C. Nguyen, M. Salamak, A. Katunin, G. Poprawa, M. Gerges, Vibration-based SHM of railway steel arch bridge with orbit-shaped image and wavelet-integrated CNN classification, Eng. Struct. 315 (2024) 118431.
[8] A. Heshmati, R.-A. Jafari-Talookolaei, P.S. Valvo, M. Saadatmorad, A novel damage detection technique for laminated composite beams under the action of a moving load, Mech. Syst. Signal Proc. 202 (2023) 110692.
[9] A. Katunin, Vibration-based spatial damage identification in honeycomb-core sandwich composite structures using wavelet analysis, Compos. Struct. 118 (2014) 385–391.
[10] B. Tefera, A. Zekaria, A. Gebre, Challenges in applying vibration-based damage detection to highway bridge structures, Asian J. Civ. Eng. 24 (6) (2023) 1875–1894.
[11] M. Saadatmorad, M.-H. Pashaei, R.-A. Jafari-Talookolaei, S. Khatir, Mode shape projection for damage detection of laminated composite plates, Math. Comput. Appl. 30 (1) (2025) 18.
[12] N.P. Raut, A. Kolekar, S. Gombi, Optimization techniques for damage detection of composite structure: a review, Mater. Today: Proc. 45 (2021) 4830–4834.
[13] Z. Wei, J. Liu, Z. Lu, Structural damage detection using improved particle swarm optimization, Inverse Probl. Sci. Eng. 26 (6) (2018) 792–810.
[14] D. Chen, Y. Li, A development on multimodal optimization technique and its application in structural damage detection, Appl. Soft Comput. 91 (2020) 106264.
[15] T. Cuong-Le, T. Nghia-Nguyen, S. Khatir, P. Trong-Nguyen, S. Mirjalili, K. D. Nguyen, An efficient approach for damage identification based on improved machine learning using PSO-SVM, Eng. Comput. 38 (4) (2022) 3069–3084.
[16] M. Saadatmorad, M. Siavashi, R.-A. Jafari-Talookolaei, M.H. Pashaei, S. Khatir, C.-L. Thanh, Genetic and particle swarm optimization algorithms for damage detection of beam-like structures using residual force method. Structural health

monitoring and engineering structures: select proceedings of SHM&ES 2020, Springer, 2021, pp. 143–157.
[17] F. Al Thobiani, S. Khatir, B. Benaissa, E. Ghandourah, S. Mirjalili, M.A. Wahab, A hybrid PSO and Grey Wolf Optimization algorithm for static and dynamic crack identification, Theor. Appl. Fract. Mech. 118 (2022) 103213.
[18] H.-L. Minh, S. Khatir, R.V. Rao, M. Abdel Wahab, T. Cuong-Le, A variable velocity strategy particle swarm optimization algorithm (VVS-PSO) for damage assessment in structures, Eng. Comput. 39 (2) (2023) 1055–1084.
[19] S. Khatir, I. Belaidi, T. Khatir, A. Hamrani, Y.-L. Zhou, M.A. Wahab, Multiple damage detection in composite beams using Particle Swarm Optimization and genetic algorithm, Mechanics 23 (4) (2017) 514–521.
[20] G.-R. Gillich, H. Furdui, M.A. Wahab, Z.-I. Korka, A robust damage detection method based on multi-modal analysis in variable temperature conditions, Mech. Syst. Signal Proc. 115 (2019) 361–379.
[21] H.A. Abdushkour, M. Saadatmorad, S. Khatir, B. Benaissa, F. Al Thobiani, A. U. Khawaja, Structural damage detection by derivative-based wavelet transforms, Arab. J. Sci. Eng. 49 (11) (2024) 15701–15709.
[22] M. Solís Muñiz, M. Algaba, P. Galvín, Continuous wavelet analysis of mode shapes differences for damage detection, Mech. Syst. Signal Proc. 40 (2) (2013) 645–666.
[23] C.P. Ratcliffe, Damage detection using a modified Laplacian operator on mode shape data, J. Sound Vib. 204 (3) (1997) 505–517.
[24] M.-B. Abdo, M. Hori, A numerical study of structural damage detection using changes in the rotation of mode shapes, J. Sound Vib. 251 (2) (2002) 227–239.
[25] P. Qiao, K. Lu, W. Lestari, J. Wang, Curvature mode shape-based damage detection in composite laminated plates, Compos. Struct. 80 (3) (2007) 409–428.
[26] I. Duvnjak, D. Damjanović, M. Bartolac, A. Skender, Mode shape-based damage detection method (MSDI): experimental validation, Appl. Sci. 11 (10) (2021) 4589.
[27] S. Umar, N. Bakhary, A.R.Z Abidin, Response surface methodology for damage detection using frequency and mode shape, Measurement 115 (2018) 258–268.
[28] M. Saadatmorad, R.-A. Jafari-Talookolaei, S. Khatir, N. Fantuzzi, T. Cuong-Le, Frugal wavelet transform for damage detection of laminated composite beams, Comput. Struct. 314 (2025) 107765.
[29] A. Katunin, J.V.A. dos Santos, H. Lopes, Damage identification by wavelet analysis of modal rotation differences, Structures 30 (2021) 1–10.
[30] J. Araujo dos Santos, A. Katunin, H. Lopes, Vibration-based damage identification using wavelet transform and a numerical model of shearography, Int. J. Struct. Stab. Dyn. 19 (04) (2019) 1950038.
[31] C. Yang, S.O. Oyadiji, Damage detection using modal frequency curve and squared residual wavelet coefficients-based damage indicator, Mech. Syst. Signal Proc. 83 (2017) 385–405.
[32] M. Saadatmorad, M.H. Shahavi, A. Gholipour, Damage detection in laminated composite beams reinforced with nano-particles using covariance of vibration mode shape and wavelet transform, J. Vib. Eng. Technol. 12 (3) (2024) 2865–2875.
[33] M.R. Papanaboina, E. Jasiuniene, E. Žukauskas, L. Mažeika, Numerical analysis of guided waves to improve damage detection and localization in multilayered CFRP panel, Mater. (Basel) 15 (10) (2022) 3466.
[34] Y. Li, M. Saadatmorad, A. Gholipour, R.-A. Jafari-Talookolaei, Optimized complex wavelet transform for damage detection in the stepped laminated composite beams, Compos. Struct. (2025) 119363.
[35] S.A. Ravanfar, H.A. Razak, Z. Ismail, S. Hakim, A hybrid procedure for structural damage identification in beam-like structures using wavelet analysis, Adv. Struct. Eng. 18 (11) (2015) 1901–1913.
[36] Y.-Y. Jiang, B. Li, Z.-S. Zhang, X.-F. Chen, Identification of crack location in beam structures using wavelet transform and fractal dimension, Shock Vib. 2015 (1) (2015) 832763.
[37] R. Nigam, S. Singh, Crack detection in a beam using wavelet transform and photographic measurements, Structures 25 (2020) 436–447.
[38] A. Katunin, Modal-based non-destructive damage assessment in composite structures using wavelet analysis: a review, Int. J. Compos. Mater. 3 (6B) (2013) 1–9.
[39] A. Katunin, Nondestructive damage assessment of composite structures based on wavelet analysis of modal curvatures: state-of-the-art review and description of wavelet-based damage assessment benchmark, Shock Vib. 2015 (1) (2015) 735219.
[40] G.R. Sahoo, J.H. Freed, M. Srivastava, Optimal wavelet selection for signal denoising, IEEE Access 12 (2024) 45369–45380.
[41] A. Katunin, R. Huňady, M. Hagara, Damage identification in composite structures using high-speed 3D digital image correlation and wavelet analysis of mode shapes, Nondestruct. Test. Eval. 40 (8) (2025) 3650–3668.
[42] A. Quarteroni, Spectral methods. Numerical models for differential problems, Springer, 2017, pp. 225–266.
[43] P. McCarthy, J. Sayre, B. Shawyer, Generalized legendre polynomials, J. Math Anal. Appl. 177 (2) (1993) 530–537.
[44] V. Antonov, K. Kholshevnikov, V.S. Shaidulin, Estimating the derivative of the legendre polynomial, Vestn. St. Petersbg. Univ.: Math. 43 (4) (2010) 191–197.
[45] G.A. Oliver, J.L.J. Pereira, M.B. Francisco, G.F. Gomes, Wavelet transform-based damage identification in laminated composite beams based on modal and strain data, Mech. Adv. Mater. Struct. 31 (19) (2024) 4575–4585.
[46] M. Saadatmorad, R.-A. Jafari-Talookolaei, H. Ghandvar, T. Cuong-Le, S. Khatir, Relative frugal wavelet transform to detect damages in functionally graded tapered beams made of porous material, Multidiscip. Model. Mater. Struct. 21 (3) (2025) 692–714.
[47] C.-Y. Tsai, S.-K. Jeng, Design of a legendre-polynomial-based orthogonal pulse generator for ultra-wideband communications, in: 2005 IEEE antennas and propagation society international symposium, 2, IEEE, 2005, pp. 680–683.
[48] X. Sun, Z. Zhang, A new finite-difference method for earthquake cycles accelerated by GPU and multigrid method, Geophys. J. Int. 241 (2) (2025) 1029–1041.
[49] G. Aklilu, S. Adali, G. Bright, Tensile behaviour of hybrid and non-hybrid polymer composite specimens at elevated temperatures, Eng. Sci. Technol. Int. J. 23 (4) (2020) 732–743.